Single-Molecule Spectroscopic Studies of Nanoscale Heterogeneity in Organically Modified Silicate Thin Films

Daniel A. Higgins,* Maryanne M. Collinson,* Ginagunta Saroja, and Angela M. Bardo

Department of Chemistry, Kansas State University, Manhattan, Kansas 66506

Received April 8, 2002. Revised Manuscript Received June 13, 2002

Single-molecule fluorescence spectroscopy is used to compare the nanoscale properties of organically modified sol−gel-derived silicate thin films prepared from different silicate precursors. Sols containing different mole fractions of isobutyltrimethoxysilane (BTMOS) and/or 3-(triethoxysilyl)propionitrile (CNS) and tetraethoxysilane (TEOS) are used for film preparation. The solvent-sensitive dye Nile red is doped into these films at nanomolar concentrations and is used to probe their nanoscale environments. The single-molecule fluorescence spectra obtained are analyzed using a form of Marcus theory for charge-transfer transitions. Important information on local film polarity and rigidity is obtained. The results show that films derived from CNS-containing sols are more polar than those prepared using BTMOS, as expected. Data obtained from a series of films as a function of film organic content (i.e., CNS or BTMOS, the remainder being TEOS) show that the local film environments become distinctly less polar and less rigid as the film organic content increases. However, the CNS and BTMOS sample series exhibit markedly different behaviors as a function of film organic content. CNS-containing materials exhibit gradual changes in their nanoscale polarity and rigidity, whereas BTMOS-containing materials exhibit a "discrete" change in these properties for films of greater than approximately 50% organic content. The latter result is attributed to phase separation and/or the formation of micelle-like domains in BTMOS-derived films. Comparisons between cohydrolyzed and separately hydrolyzed sols prepared from similar binary and ternary silane mixtures also show evidence for phase separation. Importantly, the single-molecule data indicate that the average and most common film environments are distinctly different in virtually all films studied.

I. Introduction

The sol−gel method[1] provides a convenient tool for the fabrication of inorganic and composite organic−inorganic materials.[2−5] In a typical procedure, an alkoxysilane precursor is mixed with water and a catalyst (e.g., HCl) in a mutual solvent (e.g., alcohol). Hydrolysis of the alkoxy groups and condensation of the subsequently formed silanol species begins immediately thereafter and leads initially to the formation of a viscous gel. Prior to gelation, the sol can be doped with any number of species, including organic dyes, chelating agents, and biomolecules.[2,6−8] A drop of the doped sol can then be cast onto a suitable substrate to form a thin film. Silicate films prepared using similar procedures have been used in photonic devices[9,10] and as chemical sensors[11,12] for the detection of various reagents, including H^+,[13−15] K^+ and Na^+,[16] and glucose.[17]

The sol−gel process can be used to prepare relatively "simple" silicate glasses via the hydrolysis and condensation of tetraethoxysilane (TEOS). Alternatively, more chemically and physically complex organic−inorganic hybrids can be prepared by blending TMOS with any of the numerous organoalkoxysilanes [$R-Si(OR')_3$] available.[2−5,18] These organically modified silicates are commonly known as ORMOSILs. ORMOSIL thin films have been successfully employed in the development of new chemical sensors,[5,19,20] ion-exchange coatings,[5,21]

* Corresponding authors. E-mails: higgins@ksu.edu and mmc@ksu.edu.

(1) Brinker, J.; Scherer, G. *Sol−Gel Science*; Academic Press: New York, 1989.
(2) Lev, O.; Tsionsky, M.; Rabinovich, L.; Glezer, V.; Sampath, S.; Pankratov, I.; Gun, J. *Anal. Chem.* **1995**, *67*, 22A.
(3) Schubert, U.; Husing, N.; Lorenz, A. *Chem. Mater.* **1995**, *7*, 2010.
(4) Wen, J.; Wilkes, G. L. *Chem. Mater.* **1996**, *8*, 1667.
(5) Collinson, M. M. *Trends Anal. Chem.* **2002**, *21*, 30.
(6) Avnir, D.; Braun, S.; Lev, O.; Levy, D.; Ottolenghi, M. In *Sol−Gel Optics Processing and Applications*; Klein, L. C., Ed.; Kluwer Academic Publishers: Norwell, MA, 1994; p 539.
(7) Avnir, D. *Acc. Chem. Res.* **1995**, *28*, 328.
(8) Keeling-Tucker, T.; Brennan, J. D. *Chem. Mater.* **2001**, *13*, 3331.
(9) Levy, D.; Esquivias, L. *Adv. Mater.* **1995**, *7*, 120.
(10) Reisfeld, R. *Opt. Mater.* **2001**, *16*, 1.
(11) Wolfbeis, O. S.; Reisfeld, R.; Oehme, I. *Struct. Bonding* **1996**, *85*, 51.
(12) Lin, J.; Brown, C. W. *Trends Anal. Chem.* **1997**, *16*, 200.
(13) Rottman, C.; Ottolenghi, M.; Zusman, R.; Lev, O.; Smith, M.; Gong, G.; Kagan, M. L.; Avnir, D. *Mater. Lett.* **1992**, *13*, 293.
(14) Lee, J. E.; Saavedra, S. S. *Anal. Chim. Acta* **1994**, *285*, 265.
(15) Allain, L. R.; Sorasaenee, K.; Xue, Z. *Anal. Chem.* **1997**, *16*, 2200.
(16) Kimura, K.; Sunagawa, T.; Yokoyama, M. *Anal. Chem.* **1997**, *69*, 2379.
(17) Narang, U.; Prasad, P. N.; Bright, F. V.; Ramanathan, K.; Kumar, N. D.; Malhotra, B. D.; Kamalasanan, M. N.; Chandra, S. *Anal. Chem.* **1994**, *66*, 3139.
(18) Collinson, M. M. *Mikrochim. Acta* **1998**, *129*, 149.

10.1021/cm020344j CCC: $22.00
Published on Web 07/26/2002

templated materials,[5,22] NLO devices,[23,24] and optical waveguides.[25,26]

Of utmost importance in the above applications is a detailed understanding of the chemical and physical properties of the host matrix. Particularly important are the molecular-scale polarity and rigidity properties of the individual (possibly solvent-filled) pores/cages in the host framework, the presence of host−guest interactions, and the extent of phase separation of the film components.[27] Bulk fluorescence and absorption spectroscopies have long been used to study the chemical environments surrounding organic dyes entrapped within silicate materials.[8,27−32] However, these methods typically provide information only on the "average" properties of the host matrix. They do not necessarily give detailed information about individual nanoscale chemical environments. In addition, these methods have been predominately used to study monoliths, for which the pore structure can be substantially different than that found in thin films.[1,33,34]

Single-molecule spectroscopy[35] can provide valuable new information about local chemical environments in thin-film materials. In several previous publications, we have reported studies of both organic polymer films[36] and silicate films[37−39] using different dye molecules and different single-molecule spectroscopic methods. These investigations have explored both the static and dynamic properties of film nanoenvironments. In our most recent work, we have specifically sought to develop semiquantitative methods for determining nanoscale sample polarity and rigidity properties.[36,37] We have been using a modified form of Marcus theory for charge-transfer transitions[40−43] as a means to obtain this information from single-molecule fluorescence spectra using the solvent-sensitive dye Nile red.[44] Our initial work in this area[36] describes the limitations and assumptions of the method and demonstrates its feasibility. More recently, we have applied this method to the characterization of nanoscale environments in ORMOSIL films prepared from tetraethoxysilane (TEOS) and isobutyltrimethoxysilane (BTMOS).[37] In the present paper, we seek additional information on the molecular-scale properties of ORMOSIL films prepared from mixtures of the more polar compound 3-(triethoxysilyl)-propionitrile (CNS) with TEOS. The data are compared and contrasted with those obtained from further studies of the BTMOS/TEOS system. As in our earlier publication,[37] the purpose of this study is to uncover variations in the film properties as a function of sol content alone. Because the properties of sol−gel-derived films are known to change with time[45] and with drying conditions,[38] these parameters, along with the ambient atmospheric moisture, are all held approximately constant throughout the experiments.

These studies, and their results, also help to provide a better understanding of the nanoscale solvation phenomena probed by single-molecule methods. Importantly, they demonstrate that sample-dependent differences in nanoscale polarity, rigidity, and heterogeneity can be readily explored and that new information, not readily available from bulk spectroscopic experiments, can be obtained.

II. Experimental Considerations

Samples. ORMOSIL films were prepared from tetraethoxysilane (TEOS, Aldrich, >99%), isobutyltrimethoxysilane (BTMOS, Fluka, 95%), and 3-(triethoxysilyl)propionitrile (CNS, Aldrich, 98%). A range of samples having different chemical compositions were prepared from mixtures of these starting materials (see below). In all cases, sols were prepared in 1:4:5:0.006 total silicate/ethanol/water/HCl mole ratios. Each mixture was stirred for 30 min immediately after preparation. The sols were then allowed to sit for approximately 48 h, at which point a methanolic solution of Nile red (NR) was added to yield a total dye concentration of 0.5−1 nM in the sol. NR was obtained from Aldrich and was used as received. Immediately after addition of the dye, 100 μL of the sol was spin cast onto a cleaned microscope coverslip (Fisher Premium). The resulting films were found to be 350−550 nm thick by surface profilometry (Tencor Alpha-Step 500 instrument).

Ambient atmospheric moisture is known to adsorb onto silicate surfaces[46] and in silicate devices, altering the polarity of the local environments.[26,47] During film preparation, moisture is known to affect the hydrolysis and condensation processes.[48] To minimize such effects, film preparation and characterization were performed under controlled atmospheric conditions. The films were dried in a controlled-humidity environment (34% relative humidity) for approximately 24 h prior to imaging. All single-molecule experiments were performed under dry air (20−25% relative humidity). Experiments were performed on each sample for approximately 8-h duration after they were transferred to the microscope.

(19) Rottman, C.; Turniansky, A.; Avnir, D. *J. Sol−Gel Sci. Technol.* **1998**, *13*, 17.
(20) Kimura, K.; Sunagawa, T.; Yajima, S.; Miyake, S.; Yokoyama, M. *Anal. Chem.* **1998**, *70*, 4309.
(21) Wei, H.; Collinson, M. M. *Anal. Chim. Acta* **1999**, *397*, 113.
(22) Makote, R.; Collinson, M. M. *Chem. Mater.* **1998**, *10*, 2440.
(23) Jeng, R. J.; Chen, Y. M.; Jain, A. K.; Kumar, J.; Tripathy, S. K. *Chem. Mater.* **1992**, *4*, 972.
(24) Hsiue, G.-H.; Lee, R.-H.; Jeng, R.-J. *Chem. Mater.* **1997**, *9*, 883.
(25) Sorek, Y.; Zevin, M.; Reisfeld, R.; Hurvits, T.; Ruschin, S. *Chem. Mater.* **1997**, *9*, 670.
(26) Skrdla, P. J.; Saavedra, S. S.; Armstrong, N. R.; Mendes, S. B.; Peyghambarian, N. *Anal. Chem.* **1999**, *71*, 1332.
(27) Dunn, B.; Zink, J. I. *Chem. Mater.* **1997**, *9*, 2280.
(28) Wittouck, N.; De Schryver, F.; Snijkers-Dendrickx, I. *J. Sol−Gel Sci. Technol.* **1997**, *8*, 895.
(29) Rottman, C.; Grader, G.; Avnir, D. *Chem. Mater.* **2001**, *13*, 3631.
(30) Lobnik, A.; Wolfbeis, O. S. *Analyst* **1998**, *123*, 2247.
(31) Baker, G. A.; Pandey, S.; Marziarz, E. P.; Bright, F. V. *J. Sol−Gel Sci. Technol.* **1999**, *15*, 37.
(32) Qian, G.; Yang, Z.; Yang, C.; Wang, M. *J. Appl. Phys.* **2000**, *88*, 2503.
(33) Frye, G. C.; Ricco, A. J.; Martin, S. J.; Brinker, C. J. *Mater. Res. Soc. Symp. Proc.* **1988**, *121*, 349.
(34) Brinker, C. J.; Hurd, A. J.; Schunk, P. R.; Frye, G. C.; Ashley, C. S. *J. Non-Cryst. Solids* **1992**, *147/148*, 424.
(35) Kelley, A. M. In *Encyclopedia of Chemical Physics and Physical Chemistry*; Moore, J. H., Spencer, N. D., Eds.; Institute of Physics Publishing: Bristol, U.K., 2001; Vol. 3, p 2199.
(36) Hou, Y.; Bardo, A. M.; Martinez, C.; Higgins, D. A. *J. Phys. Chem. B* **2000**, *104*, 212.
(37) Bardo, A. M.; Collinson, M. M.; Higgins, D. A. *Chem. Mater.* **2001**, *13*, 2713. Bardo, A. M.; Collinson, M. M.; Higgins, D. A. *Chem. Mater.* **2001**, *13*, 3058.
(38) Mei, E.; Bardo, A. M.; Collinson, M. M.; Higgins, D. A. *J. Phys. Chem. B* **2000**, *104*, 9973.
(39) Wang, H.; Bardo, A. M.; Collinson, M. M.; Higgins, D. A. *J. Phys. Chem. B* **1998**, *102*, 7231.
(40) Marcus, R. A. *J. Chem. Phys.* **1965**, *43*, 1261.
(41) Marcus, R. A. *J. Phys. Chem.* **1989**, *93*, 3078.
(42) Marcus, R. A. *J. Phys. Chem.* **1990**, *94*, 4963.
(43) Brunschwig, B. S.; Ehrenson, S.; Sutin, N. *J. Phys. Chem.* **1987**, *91*, 4714.
(44) Deye, J. F.; Berger, T. A.; Anderson, A. G. *Anal. Chem.* **1990**, *62*, 615.
(45) Dunbar, R. A.; Jordan, J. D.; Bright, F. V. *Anal. Chem.* **1996**, *68*, 604.
(46) Garbatski, U.; Folman, M. *J. Phys. Chem.* **1956**, *60*, 793.
(47) Rottman, C.; Avnir, D. *Proc. SPIE* **2000**, *3943*, 154.
(48) Collinson, M. M.; Wang, H.; Makote, R.; Khramov, A. *J. Electroanal. Chem.* **2002**, *519*, 65.

The samples investigated include those prepared from cohydrolyzed and separately hydrolyzed silicate precursors.[49] The cohydrolyzed systems were prepared by mixing all silicate precursors at the start of sol preparation. Treatment of these sols and subsequent sample preparation were exactly as described above. Films were prepared from cohydrolyzed sols of 10, 25, 33, 50, and 67% organic precursor (BTMOS or CNS) content. In each case, TEOS comprised the remaining silicate (i.e., the sols above were 90, 75, 67, 50, and 33%, respectively, in TEOS). Separately hydrolyzed systems were prepared by first making several individual sols from individual (pure) silanes. The individual sols were allowed to sit separately for 48 h. At the end of this period, dye was added to each sol, the sols were mixed in the appropriate ratios, and the films were cast. Binary mixtures of separately hydrolyzed inorganic and organic precursors were prepared to yield sols of 50% organic content. Finally, ternary mixtures incorporating 25% BTMOS, 25% CNS, and 50% TEOS were also prepared. These materials were prepared as both cohydrolyzed and separately hydrolyzed sols. In the latter samples, two versions of the separately hydrolyzed materials were employed. In one, all three components were prepared as separate sols. For the other, separately prepared 50% BTMOS/TEOS and 50% CNS/TEOS sols were mixed just prior to film casting.

All films are designated below by the BTMOS and/or CNS content of the sols used in their preparation. It is understood that TEOS comprises the remaining silicate (up to 100%) content. For example, a film prepared from a sol containing equal amounts of CNS and TEOS is referred to simply as a 50% CNS film, although it is likely that no CNS monomers remain in the film after spin casting.

Instrumentation. All single-molecule studies were performed on a sample scanning confocal microscope.[36,39] This system was constructed around an inverted, epi-illumination microscope (Nikon TE-200). Light from a green helium/neon laser (543 nm) was used to excite the single molecules. The excitation beam was first passed through polarization control optics, a 543-nm band-pass filter (CVI, 10-nm passband), and a telescope, prior to being directed into the epi-illumination port of the microscope. A dichroic beam splitter (Chroma 565DCLP) was used to reflect the light into the microscope objective. The beam size was adjusted to fill the back aperture of the objective, a 1.3 NA, 100× oil immersion objective (Nikon Plan Fluor). This system produced a nearly diffraction-limited spot of approximately 300-nm diameter in the sample. The sample was mounted above the objective on a piezoelectric scanning stage (Queensgate) employing closed-loop *X*,*Y* feedback. Software written in-house was used to control the stage and to collect images.

The fluorescence emitted by the single molecules was collected by the oil immersion objective. All emission to the red of 565 nm passed back through the dichroic beam splitter and into the detection path of the microscope. Single-molecule emission was further isolated from residual laser light by passing it through a 543-nm holographic notch filter (Kaiser Optical). Band-pass filters having a 100-nm band-pass centered at 600 and 650 nm were employed separately in different experiments to help minimize the background counts in the images. A single-photon-counting avalanche diode was used as the detector. The fluorescence signal was integrated for 40 ms/pixel in the 100 × 100 pixel images collected in these studies.

Fluorescence spectra were recorded by sending the single-molecule fluorescence directly (without the use of band-pass filters) into the entrance slit (∼150 μm) of an imaging spectrograph (Acton Research). The fluorescence was detected with a back-thinned, liquid-N_2-cooled CCD detector (Roper Scientific). The wavelength axis was calibrated using a neon lamp. A standardized tungsten/halogen lamp was used to determine the wavelength-dependent transmission and detection efficiency for the entire optical system. All spectra were corrected for these results. Fluorescent polystyrene microspheres were employed to verify microscope alignment on a daily basis. The emission maximum observed for the spheres varied by no more than ±2.5 nm. Such variations arise from slight variations in the optical alignment of the instrument.

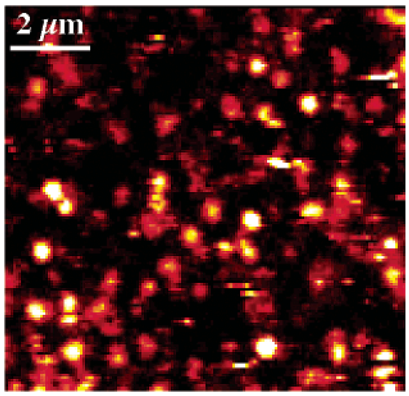

Figure 1. Typical fluorescence image of an ORMOSIL film (67% CNS) doped with NR. The NR concentration in the sol was 0.5 nM.

III. Results and Discussion

Imaging Experiments. Single-molecule data collection begins with the recording of fluorescence images of small sample regions. Figure 1 shows a representative image of a 10 μm × 10 μm area in a NR-doped 67% CNS film. As has been discussed previously, such images provide initial, qualitative information on local sample properties.[36−38] Single molecules entrapped at fixed locations (on the time scale of the experiment) usually yield round spots in the fluorescence images. However, fluorescent "streaks" are also observed in some images (see Figure 1).[37] These streaks are short segments of individual linescans that exhibit fluorescence well above the background. They arise from dramatic fluctuations in the emission characteristics of the single molecules. Among other possibilities, the molecules might "blink" on and off on long time scales,[50−53] or their emission yields might vary.[36,54] The fluctuations might also arise from molecules moving (rotating and translating) rapidly within the sample region being imaged.[37,55−58] The relative number of spots and streaks observed in a given image is a strong function of the relative amounts of organic and inorganic silicate precursors used in sol preparation.[37]

Films of greater than 67% organic content (i.e., CNS or BTMOS) generally yield images with a predominant number of streaks. Although some round spots are still observed in films of higher organic content, these are

(49) Brennan, J. D.; Hartman, J. S.; Ilnicki, E. I.; Rakic, M. *Chem. Mater.* **1999**, *11*, 1853.

(50) Ha, T.; Enderle, T.; Chemla, D. S.; Selvin, P. R.; Weiss, S. *Chem. Phys. Lett.* **1997**, *271*, 1.

(51) Dickson, R. M.; Cubitt, A. B.; Tsien, R. Y.; Moerner, W. E. *Nature* **1997**, *388*, 355.

(52) Yip, W.-T.; Hu, D.; Yu, J.; Vanden Bout, D. A.; Barbara, P. F. *J. Phys. Chem. A* **1998**, *102*, 7564.

(53) Weston, K. D.; Carson, P. J.; DeAro, J. A.; Buratto, S. K. *Chem. Phys. Lett.* **1999**, *308*, 58.

(54) Weston, K. D.; Carson, P. J.; Metiu, H.; Buratto, S. K. *J. Chem. Phys.* **1998**, *109*, 7474.

(55) Schmidt, T.; Schütz, G. J.; Baumgartner, W.; Gruber, H. J.; Schindler, H. *Proc. Natl. Acad. Sci. USA* **1996**, *93*, 2926.

(56) Dickson, R. M.; Norris, D. J.; Tzeng, Y.-L.; Moerner, W. E. *Science* **1996**, *274*, 966.

(57) Wirth, M. J.; Swinton, D. J. *Anal. Chem.* **1998**, *70*, 5264.

(58) Ha, T.; Glass, J.; Enderle, T.; Chemla, D. S.; Weiss, S. *Phys. Rev. Lett.* **1998**, *80*, 2093.

believed to represent a minority of the total population of single molecules. The streaks observed in these samples are clearly a result of rapid molecular diffusion through or on the films.[37] Strong evidence for such a conclusion is obtained by recording the total fluorescence from a single location for long periods of time.[37,57] In regions exhibiting streaks, these "fluorescence transients" show rapid fluctuations in the emission signal but no evidence of photobleaching on time scales of more than 10 minutes.[37] Such behavior indicates that the fluorescence comes from several single molecules diffusing (usually one at a time) in and out of the microscope focus. Such fast molecular diffusion is a clear indicator of the relatively more "fluid" nature of the environments in ORMOSIL films.[28,37]

Fluorescence Spectroscopy. Fluorescence spectra recorded from the single molecules provide an alternative and more quantitative means for characterizing local film[36,37,59] and surface[54] properties. Such studies are the primary focus of this publication. In these experiments, the single molecules located in imaging experiments are positioned one at a time in the microscope focus, and their spectra are recorded. Their emission maxima, ν_{fl}, and emission bandwidths, $\delta\nu_{fl}$, are then used to better understand the polarity and rigidity properties of the local film environments.

Only certain films can be characterized by single-molecule fluorescence spectroscopy. Again, only those exhibiting a predominance of round fluorescent spots are suitable. In other situations, the results obtained would be biased toward molecules entrapped at fixed sites. As a result, samples of greater than 67% organic content were not studied in the present experiments. As described previously,[37] films of pure TEOS must also be excluded, because of the extremely weak fluorescence obtained (i.e., few fluorescent spots are observed) from NR. Weak NR emission is likely a result of the profound red shift in its excitation spectrum[36] and the dramatic reduction in its emission yield[60] in polar materials. As a result, single-molecule data collected from samples of nearly pure TEOS are biased toward the most fluorescent molecules in the least polar environments. For these samples, the single-molecule data do not adequately reproduce the bulk spectrum when summed.[37] The full range of samples characterized by single-molecule spectroscopy were prepared from sols ranging from 10 to 67% in organic precursor content. Unfortunately, there is some inherent bias toward the least polar environments even in these data, for the reasons mentioned above. However, as shown previously,[37] the single-molecule data very closely reproduce the bulk data in this range of samples, suggesting that the bias is negligible.

Several hundred single-molecule fluorescence spectra were recorded for each of the samples studied. Weak spectra (i.e., those exhibiting peak fluorescence signals of less than twice the background) were eliminated. The remaining spectra were fit with two or three Gaussian functions, as necessary.[54] Figure 2 shows two representative spectra and their fits. The quality of each fit is

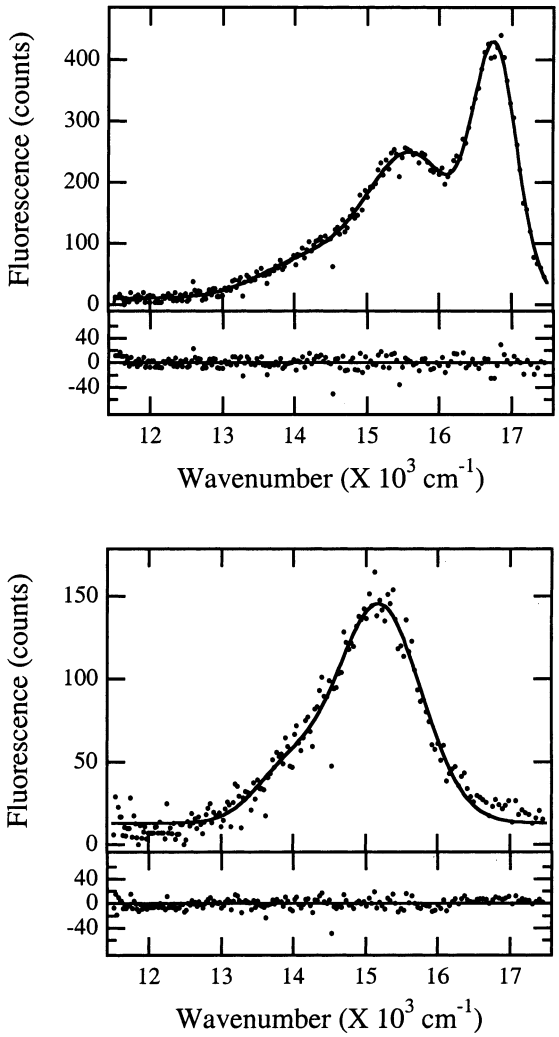

Figure 2. Representative single-molecule fluorescence spectra recorded for NR in ORMOSIL thin films. Also shown are fits to these spectra. In most cases, the spectra could be fit well with two Gaussian functions (bottom). In a few cases, three Gaussians were required (top). The residuals shown at the bottom of each set depict the goodness of the fits. Important parameters taken from these fits are the emission maximum, ν_{fl}, and the fwhm of the highest-energy band, $\delta\nu_{fl}$.

evidenced by the fit residuals, also shown in Figure 2. All parameters, except for the spacings of the Gaussian functions (corresponding to the vibronic band separations), were allowed to float freely in the fitting procedure. The vibronic band spacings were constrained to fall in the 1100−1700 cm^{-1} range. Without such constraint, the broadest spectra, for which the vibronic structure was completely obscured, yielded uncertain fitting parameters. All spectra that exhibited distinct vibronic structure could be fit well within these constraints. The peak position, ν_{fl}, of the vibronic band centered at highest energy (i.e., the electronic origin) was used in the analysis presented below, along with its full-width-at-half-maximum (fwhm), $\delta\nu_{fl}$. Histograms of the raw spectral data (ν_{fl} and $\delta\nu_{fl}$) obtained for each sample have been provided as Supporting Information.

The spectroscopic parameters obtained were used in a modified Marcus analysis[40−43] described previously.[36,37] Briefly, each molecule's emission maximum (ν_{fl}) is related to the equilibrium free energy of its electronic transition, $\Delta G°$, and the local reorganiza-

(59) Blum, C.; Stracke, F.; Becker, S.; Müller, K.; Meixner, A. J. *J. Phys. Chem. A* **2001**, *105*, 6983.
(60) Dutta, A. K.; Kamada, K.; Ohta, K. *J. Photchem. Photobiol. A* **1996**, *93*, 57.

tion energy, λ, as follows

$$\nu_{fl} = \Delta G° - \lambda = \Delta G°_v - \Delta\Delta G° - \lambda \quad (1)$$

In eq 1, $\Delta G°_v$ is the free energy of the transition in the absence of any solvent (i.e., in a vacuum). $\Delta G°_v$ has been estimated previously to be 20 600 cm^{-1} for NR.[36] $\Delta\Delta G°$ is the solvent-induced shift in the transition energy. The parameter λ represents the total reorganization energy of the molecule and its immediate surroundings in a relatively solid sample.[42] Under these circumstances, it is assumed that many of the solute (single-molecule) and solvent (environment) motions are restricted, or frozen, on a time scale much longer than the excited-state lifetime of the molecule. Marcus has discussed how such "frozen" samples can be modeled in a recent publication.[42]

The reorganization energy of each molecule is determined from the fwhm of its emission peak[41]

$$\delta\nu_{fl} = 4\sqrt{(\ln 2)\lambda kT} \quad (2)$$

In eq 2, k is the Boltzmann constant, and T is the temperature. As noted above, $\delta\nu_{fl}$ represents the fwhm of a single vibronic band. Therefore, λ represents the reorganization energy associated with the unfrozen low-frequency nuclear motions of the molecule and its environment. One limitation of eq 2 is that the entire vibronic bandwidth is attributed to dynamics occurring on a time scale shorter than the excited-state lifetime. It is well-known that spectral diffusion phenomena[61−63] can also contribute to the observed widths. On time scales greater than ~100 ms for dry samples, it appears that spectral diffusion contributes no more than 100−200 cm^{-1} to the individual widths. Unfortunately, it is not possible at present to determine the contributions of spectral diffusion on submicrosecond to millisecond time scales.

As a final caveat, it should be noted that Marcus' model for solvation processes in frozen environments assumes that the environment surrounding the ground-state solute is in its equilibrium configuration. For such frozen samples, a reduction in λ is accompanied by an increase in the transition energy.[42] Others have observed such an effect and aptly named it "rigidochromism".[64,65] However, as noted in our previous publications,[36,37] and as is the case here, we assume that the system is frozen in a nonequilibrium configuration. In this case, it is assumed that both the ground and excited states are shifted to higher energies by similar amounts. Hence, the frozen environmental dipoles do not contribute to the transition energy. If such a model were inappropriate, molecules exhibiting small λ values would also yield small $\Delta\Delta G°$ values (reflecting the expected blue shift in the emission due to rigidochromism). As shown below, the opposite trend is actually observed, providing support for our modifications to the theory.

The $\Delta\Delta G°$ and λ parameters derived from the single-molecule spectroscopic data and the model outlined above are then used to describe the polarity and rigidity properties, respectively, of the nanoscale environments in the silicate samples.

Average Sample Properties. Figure 3 shows histograms of the $\Delta\Delta G°$ and λ values obtained for the range of samples (binary silicate mixtures) studied. The data show clear, monotonic trends with sample composition. These trends are most clearly depicted by the average values for $\Delta\Delta G°$ and λ obtained from each sample. These averages were not taken from the histograms but rather were obtained by summing the single-molecule $\Delta\Delta G°$ and λ values and dividing by the number of spectra in each set. The values obtained are distinct from the histogram peaks (see below). Plots of these averages are shown in Figure 4. In both the CNS and BTMOS sample series, the measured λ values are smallest for samples of highest TEOS content and largest for those of high organic content. Such results reflect an increase in the average reorganization energy with increasing film organic content. From well-known dielectric continuum models (applicable to solution-phase systems),[43,66] an opposite trend is expected for liquid samples of otherwise identical composition. The reduced polarity expected for the CNS and BTMOS materials would yield a smaller reorganization energy. However, such continuum models are not broadly applicable to single-molecule studies of "solid" materials.

In the present situation, where many molecular and solvent motions are effectively frozen, very different effects are obviously observed. The observed increase in reorganization energy with increasing organic content is clearly a result of the "freeing" of molecular and environmental motions. As has been described previously,[28,37] the environments within silicate materials incorporating organically functionalized silanes are expected to be more fluid. The greater fluidity of the environments in these materials results, in part, from a reduction in the extent of cross-linking that occurs between silicate species. The organically functionalized silicates have fewer reactive Si−OR groups, whereas TEOS can form up to four Si−O−Si linkages. Hence, as we have proposed previously,[37] λ can more appropriately be taken to reflect the fluidity of the molecular-scale environments found in these materials. More fluid environments (as distinct from those that are simply more polar) then yield larger λ values. It can thus be concluded that the fluidity of the nanoscale environments in each of the CNS and BTMOS sample series increases with increasing organic content.

However, a comparison of the λ values between the CNS and BTMOS sample series indicates that environmental fluidity is not the only factor governing the results. The λ values obtained for the CNS samples are clearly larger than those obtained for BTMOS samples of equivalent compositions. On average, the difference is approximately 260 cm^{-1}. This observation is particularly noteworthy because both sample series use trifunctional organically modified precursors. The extent of cross-linking in the silicate matrixes should then be similar for CNS and BTMOS samples of similar organic

(61) Ambrose, W. P.; Moerner, W. E. *Nature* **1991**, *349*, 225.
(62) Lu, H. P.; Xie, X. S. *Nature* **1997**, *385*, 143.
(63) Kettner, R.; Tittel, J.; Basche, T.; Bräuchle, C. *J. Phys. Chem.* **1994**, *98*, 6671.
(64) Wrighton, M.; Morse, D. L. *J. Am. Chem. Soc.* **1974**, *96*, 998.
(65) McKiernan, J.; Pouxviel, J.-C.; Dunn, B.; Zink, J. I. *J. Phys. Chem.* **1989**, *93*, 2129.
(66) Lakowicz, J. R. *Principles of Fluorescence Spectroscopy*, 2nd ed.; Plenum Press: New York, 1999.

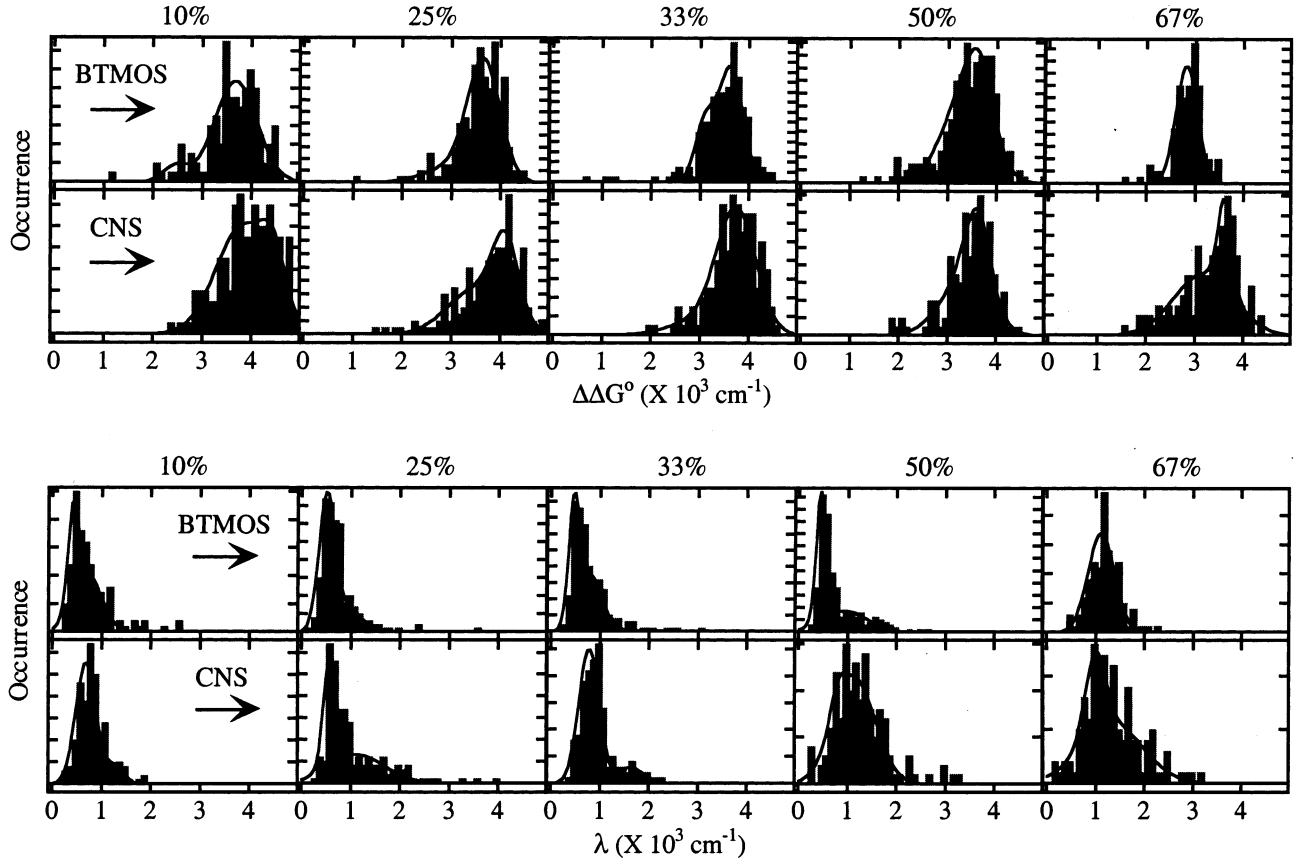

Figure 3. Histograms of the transition energy red shift (relative to that in a vacuum), $\Delta\Delta G°$ (top pair of rows), and of the reorganization energy, λ (bottom pair of rows), for NR in films prepared from sols containing BTMOS (top row in pair) and CNS (bottom row in pair). The vertical axis in each histogram gives the number of occurrences for each value. The tick marks for the $\Delta\Delta G°$ data denote increments of 2. Those for the λ data denote increments of 5. Data for films composed of 10, 25, 33, 50, and 67% organic modifier are shown. Also shown are double-Gaussian fits to the histograms. The fitted data were used only to determine the peak of each distribution.

contents. In a qualitative sense, the BTMOS and CNS sample series should have similar rigidity properties. The above observations result because λ also incorporates information on sample polarity differences, as expected from continuum models.[43,66] The differences observed between the CNS and BTMOS sample series are then attributable, on average, to polarity (rather than rigidity) differences. Indeed, interpretation of the measured λ values in terms of local environmental rigidity alone is made more difficult by such polarity effects. In the BTMOS sample series, the polarity of the material decreases, and its fluidity increases with increasing organic content. These two properties have opposite effects on λ. It is clear that changes in environmental rigidity dominate over polarity effects in this sample series as λ is observed to increase substantially in films of high BTMOS content. In the CNS samples, the difference in polarity between CNS and TEOS is less pronounced. As a result, polarity changes play less of a role in the λ data. The gradual increase in λ with increasing CNS content is, therefore, a clear indicator of increased environmental fluidity.

The $\Delta\Delta G°$ values obtained in the above analysis are interpreted to reflect the polarity of the local environments.[36,37] The measured values describe the transition energy after the system has relaxed to its equilibrium configuration. More polar environments yield larger $\Delta\Delta G°$ values. In contrast to the measured λ values, the rigidity of the environment is not expected to contribute to the measured $\Delta\Delta G°$ value. Were $\Delta\Delta G°$ strongly dependent on sample rigidity, then small $\Delta\Delta G°$ values would be expected for samples with small λ values. Exactly the opposite is observed, as depicted by the data in Figure 4. These data indicate that the samples in each series become less polar as more organic functionality (BTMOS or CNS) is incorporated into the films. The data also show that the CNS samples are more polar on average than their BTMOS counterparts, as expected.

It should be noted that the specific effects of silicate matrix polarity and rigidity cannot be separated from the influence of any residual solvent (i.e., water) present in these films. Because of the different chemical compositions of the films, the amount of residual solvent is likely correlated with precursor composition as well. The more polar samples of low organic content might contain more water that might also be hydrogen-bonded to the matrix. A relatively more polar, less fluid environment would result, as observed. Films of higher CNS content, because of their greater polarity, might be relatively more hydrated than films prepared from BTMOS-containing sols. In this instance, relatively more (free) water might be present in the CNS series of samples, yielding more polar, more fluid environments, as depicted in the data.

Initial information on composition-dependent variations in the nanoscale sample properties can also be obtained from the trends observed in the average film

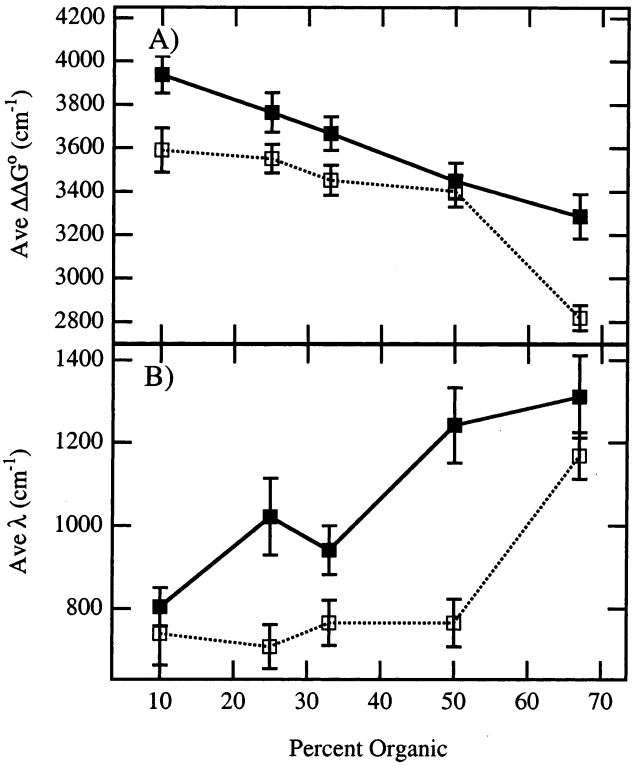

Figure 4. (A) Average $\Delta\Delta G°$ values for the CNS (filled squares) and BTMOS (open squares) data sets shown in Figure 3. (B) Average λ values for the CNS (filled squares) and BTMOS (open squares) data sets shown in Figure 3. The error bars in A and B represent the 95% confidence intervals for the mean in each sample.

properties. For example, both the $\Delta\Delta G°$ and λ data for the CNS series show that relatively gradual changes in film properties occur as more organic functionality is incorporated into the films. Indeed, an almost linear dependence of $\Delta\Delta G°$ and λ on organic content is observed. In contrast, for the BTMOS sample series, little change in these parameters is observed for the four films of lowest organic content. A dramatic change in both the $\Delta\Delta G°$ and λ is then observed for the 67% BTMOS sample. In our previous publication,[37] data obtained from 75% BTMOS materials was shown to fit well within this trend. The results point to an apparently discrete change in the nanoscale film properties for samples of approximately 50% BTMOS content. Such behavior might result from phase separation of TEOS-rich and BTMOS-rich domains. Although the exact nature of such phase separation is unknown, it might involve the formation of micellar-like regions, as originally proposed by Avnir and co-workers.[29,67] Because NR is a hydrophobic dye, it is expected to partition preferentially into regions of high organic content. Therefore, the abrupt change in film properties is actually believed to result from BTMOS and TEOS phase separation, coupled with partitioning of the dye into the resulting BTMOS-rich domains.

The much more gradual changes observed for the CNS sample series contrast strongly with the BTMOS data. The differences between these samples are likely a result of the much greater miscibility of the CNS and TEOS precursors. Their greater miscibility results from the presence of the polar carbonitrile group on CNS. On the basis of the data obtained, it is then proposed that the CNS and TEOS remain well mixed on molecular length scales throughout the range of samples studied.

Nanoscale Sample Properties. Whereas the average film data discussed above yield important insight into silicate film properties, from a chemical perspective the properties of the most common nanoscale environments are more important. In samples for which random variations in the environmental properties lead to Gaussian-shaped inhomogeneous distributions, the average film environments are, in fact, the most common film environments. In other situations, the average and most common environments might differ dramatically. A closer look at Figure 3 shows that the distributions are not Gaussian in shape. Hence, as with the results of bulk spectroscopic experiments, the above interpretations of the average λ and $\Delta\Delta G°$ values can provide a misleading view of overall sample properties. Single-molecule data provide much better information in this respect, via the probing of individual nanoscale film environments. Importantly, the single-molecule results demonstrate that the heterogeneity in these materials is not simply due to random variations in the molecular-scale environments; otherwise, Gaussian-shaped distributions would be observed.

Information on the most common environments found in these films can be obtained by simply determining the peak position for each distribution (see Figure 3). Unfortunately, it is difficult to determine the exact peak in each case because of noise in the histograms. The peak values were determined here by curve fitting. For lack of better information on how these data should be fit, multiple Gaussian functions were employed. The peak positions for each $\Delta\Delta G°$ and λ distribution obtained in this analysis are plotted in Figure 5, along with the corresponding average values for each sample. Such an analysis is consistent with the existence of multiple classes of environments in these films that are broadened by random variations in their properties. Should these variations be nonrandom, fitting with Gaussian functions would not be strictly appropriate.

The peaks in the λ histograms for the 10% BTMOS and 10% CNS samples yield values of 400 and 700 cm^{-1}, respectively. Again, the higher peak λ value obtained for the CNS sample is expected from the polarity arguments presented above. This trend is generally maintained in films of increasing organic content. However, the peak λ values for the 67% CNS and 67% BTMOS samples are approximately the same (1020 and 1100 cm^{-1}, respectively). These values suggest that the most common environments in the BTMOS and CNS samples of high organic content have similar properties. Again, as shown in Figure 4, the average λ value for the CNS sample is much larger than that for BTMOS. The greater average polarity of the CNS materials clearly results from the incorporation of environments of distinctly greater polarity in the films. These more polar environments are reflected in the much larger and longer tail to higher λ values observed in the histogram for the 67% CNS sample.

The appearance of the λ distribution peaks at similar values for these two samples (67% organic content) suggests that they differ in *both* their polarity and

(67) Frenkel-Mullerad, H.; Avnir, D. *Chem. Mater.* **2000**, *12*, 3754.

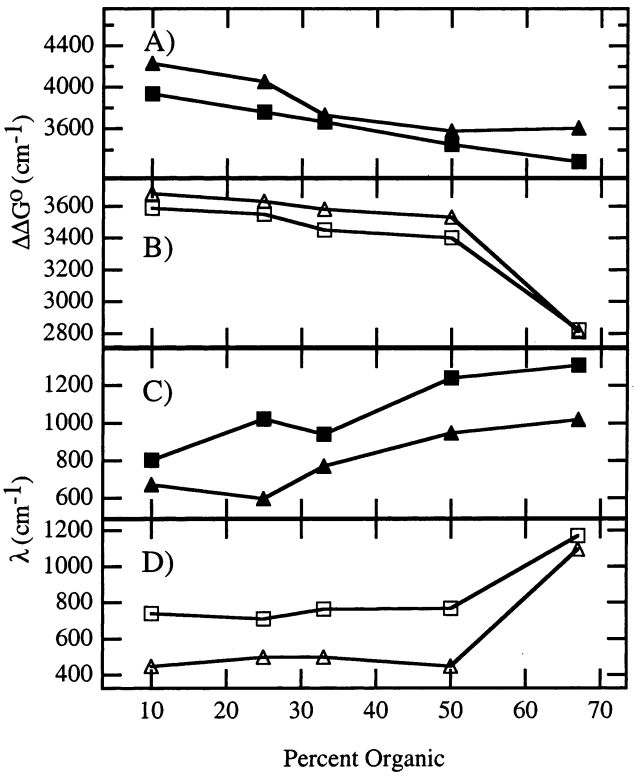

Figure 5. (A,B) Comparisons of the average (squares) and peak (triangles) $\Delta\Delta G°$ distribution values for (A) CNS and (B) BTMOS samples. (C,D) Comparisons of the average (squares) and peak (triangles) λ distribution values for (C) CNS and (D) BTMOS samples. The error bars on the distribution peak values are similar to those on the average values (i.e., 100 cm^{-1}).

rigidity properties. Because the CNS-functionalized precursor is clearly more polar than its BTMOS counterpart, it must be concluded that the 67% CNS film environments are also more rigid than the environments in the corresponding BTMOS films. Otherwise, the λ distribution for the CNS samples would be peaked at higher values than that for the BTMOS materials. On the λ scale, the polarity and rigidity attributes must then fortuitously shift the CNS data into correspondence with the BTMOS data. The apparent complexity in the differences between the CNS and BTMOS samples is again attributed to the different miscibilities of the organic precursors with TEOS. Environments composed of molecularly mixed CNS and TEOS materials are expected to be both more rigid and more polar than the BTMOS-rich environments found in films of high BTMOS content. In the BTMOS samples, phase separation of BTMOS and TEOS materials, coupled with partitioning of the dye into the BTMOS-rich domains, leads to the observation of relatively more fluid, less polar environments.

The $\Delta\Delta G°$ distributions provide valuable additional evidence as to the nanoscale origins of polarity differences in the CNS and BTMOS materials. In contrast to the λ distributions, the $\Delta\Delta G°$ distributions for the majority of the BTMOS samples appear to be more Gaussian in nature. The CNS samples, however, yield a predominance of distributions skewed toward higher $\Delta\Delta G°$ values. Indeed, the peaks in the $\Delta\Delta G°$ histograms occur at larger values for the majority of CNS samples. This is the expected result and reflects the greater polarity of the CNS materials. However, the CNS histograms also incorporate long tails to smaller values. These tails point to the presence of minority environments of similar polarities in the CNS and BTMOS samples. These tails are also important because they lead to an overall reduction in the average polarity of each film. They likely result from the presence of frozen environments having distinctly nonequilibrium solvation properties. Because the CNS materials are more polar, a wider range of environments having different polarities can be frozen in. The increased width of the $\Delta\Delta G°$ distributions for the CNS samples that result then reflect the greater heterogeneity of the CNS materials in terms of their polarity.

It is particularly interesting that, whereas the $\Delta\Delta G°$ distributions for the CNS samples are mostly peaked at larger values than those of their BTMOS counterparts, the 50% BTMOS and CNS samples yield very similar peak values (see Figures 3 and 5). This deviation in the apparent trend is due entirely to the abrupt change in the BTMOS film environments that occurs near the 50% BTMOS level. Indicative of this change is the much larger distribution width observed for the 50% BTMOS sample relative to those of other samples of high organic content. The greater width of this distribution again might be due to phase separation of the BTMOS and TEOS materials. A second class of environments having distinctly lower polarities is formed as the BTMOS content of the films is increased to around 50%.

The possible role played by hydrogen bonding in the observation of such bimodal distributions has been discussed previously.[37] Hydrogen bonding between NR and surface silanol groups is believed to lead to an increase in $\Delta\Delta G°$.[37] As the film organic content increases, fewer silanol groups are available for hydrogen bonding. A dramatic reduction in the local concentration of such silanol groups occurs along with phase separation of the inorganic and organic film components, possibly contributing to the discrete changes observed in $\Delta\Delta G°$ for the BTMOS sample series. λ is not expected to be directly influenced by hydrogen bonding. However, because λ effectively reflects the organic content of the local environment, its value will correlate with the extent of hydrogen bonding. It will be much smaller in TEOS-rich regions favoring hydrogen bonding and much larger in organic-rich regions where hydrogen bonding is less prevalent.

While CNS and TEOS are believed to remain molecularly mixed, there is also evidence for the presence of (at least) two classes of environments in the CNS samples. The apparently bimodal distributions in $\Delta\Delta G°$ and λ are likely due to variations in the extent of hydrogen bonding. As in the BTMOS samples, hydrogen bonding directly influences the observed $\Delta\Delta G°$ values and can also indirectly affect λ. Smaller $\Delta\Delta G°$ values and larger λ values are expected for non-hydrogen-bonded NR. As no clear evidence for phase separation exists in the CNS data, the effects of hydrogen bonding are expected to be observed throughout the range of samples studied. As organic functionality is incorporated in the films, the environments gradually become more fluid (i.e., more "open") and less polar. Both hydrogen-bonded and nonbonded NR molecules show the gradual

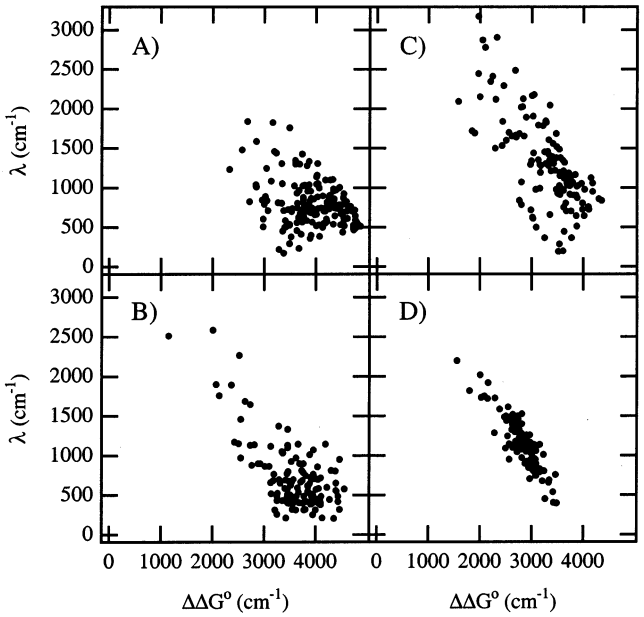

Figure 6. Correlation plots prepared from the individual λ and $\Delta\Delta G°$ values used in the histograms shown in Figure 3. Plots for samples of (A) 10% CNS, (B) 10% BTMOS, (C) 67% CNS, and (D) 67% BTMOS are shown. An overall negative correlation between λ and $\Delta\Delta G°$ is reflected in the data. Also depicted is the more profound heterogeneity of the CNS samples, relative to that of the films containing BTMOS.

changes in environmental polarity and rigidity. Hence, bimodal distributions appear throughout the range of samples studied.

Overall Sample Heterogeneity. The discussion presented above explores the specific origins of ORMOSIL heterogeneity. In many instances, observed variations in film properties were attributed to the presence of a few classes of chemically distinct environments.[27] However, it is more reasonable to assume that many different environments are formed in these materials. As a result, it is also instructive to compare the overall degree of heterogeneity between the various samples. Here, correlation plots of λ versus $\Delta\Delta G°$ are used to better depict material heterogeneity. Examples of these plots are shown in Figure 6.

In films of low organic content, there is substantial scatter in the data for both CNS and BTMOS samples. Aside from the slight differences in polarity and rigidity of these materials discussed above, the distributions shown in Figure 6A and B are quite similar. The film environments in both samples are predominantly controlled by TEOS. Substantial variability results from the range of possible chemical configurations that can occur in the nanoscale environments of TEOS-derived samples.[37]

In films of high organic content, dramatic differences are observed between the BTMOS and CNS samples, as shown in Figure 6C and D. The scatter in the BTMOS film data is dramatically less than that for the film of low BTMOS content. The apparent reduction in heterogeneity for the 67% BTMOS sample again likely reflects phase separation of BTMOS-rich and TEOS-rich domains. Coupled with partitioning of NR into the BTMOS-rich regions, these data then reflect the apparent homogeneity of the BTMOS-rich environments.

In stark contrast to the BTMOS data, the CNS films remain relatively inhomogeneous across the entire range of samples studied. These observations are consistent with molecular-scale mixing of the polar TEOS and CNS film components. The wide range of possible chemical environments that can form in these materials is observed throughout the range of samples studied. However, some subtle differences in the CNS data scatter are observed in Figure 6. The data reflects increased variability in λ, indicating that sample heterogeneity is more dynamic in character for films of high CNS content.

Cohydrolyzed vs Separately Hydrolyzed Samples. To further explore the effects of film-component phase separation, films designed to incorporate phase-separated domains were also prepared and characterized. Phase-separated materials were prepared by separate hydrolysis and condensation of the silicate precursors.[49] In this procedure, sols of "pure" BTMOS, CNS, and TEOS were prepared in separate vessels and were combined immediately prior to film casting. Final film composition is then only partly determined by the miscibility of the sols. It is also controlled by the mixing time and method employed. Single-molecule spectroscopic results from these separately hydrolyzed materials are shown in Figure 7. Also shown are the results obtained from identical cohydrolyzed materials. Films prepared from both binary (CNS and TEOS or BTMOS and TEOS) and ternary (BTMOS, CNS, and TEOS) sol mixtures were characterized.

Single-molecule data are difficult to obtain from the separately hydrolyzed films. As mentioned above, materials prepared from sols of high organic content show strong evidence for fast molecular diffusion. Because films prepared from separately hydrolyzed sols are expected to incorporate organic-rich domains, it is not surprising that some regions in these films show the same streaks observed in other films of high organic content. Figure 7A shows a representative image of a sample prepared by mixing separately hydrolyzed CNS, BTMOS, and TEOS in a 1:1:2 ratio. The upper left half of the image shows predominantly round fluorescent spots, whereas the lower right shows substantial image streaking.

Time-dependent emission transients recorded for individual spots in the upper left part of the image exhibit approximately constant emission (neglecting fluctuations due to shot noise). After a few tens of seconds, each transient undergoes a discrete drop in signal to the background level. No signal recovery is usually observed. Such data are consistent with single-molecule emission, terminated by photochemical bleaching. In contrast, the emission transients from single points in the lower right part of the image (Figure 7A) exhibit dramatic signal fluctuations between a wide range of nonzero levels and the background level. Importantly, no final photobleaching transitions are observed in such transients recorded over periods as long as 10 min. The behavior in the region exhibiting image streaks is clearly consistent with rapid translational diffusion of single molecules within these film regions.[37,57] The absence of a clear photobleaching event indicates that new molecules must be continuously moving into the focal volume of the microscope. Of course, the molecules are also rotating, and these motions will also contribute to the fluctuations.[58] Regardless of the exact mechanism by which the signals fluctuate, the

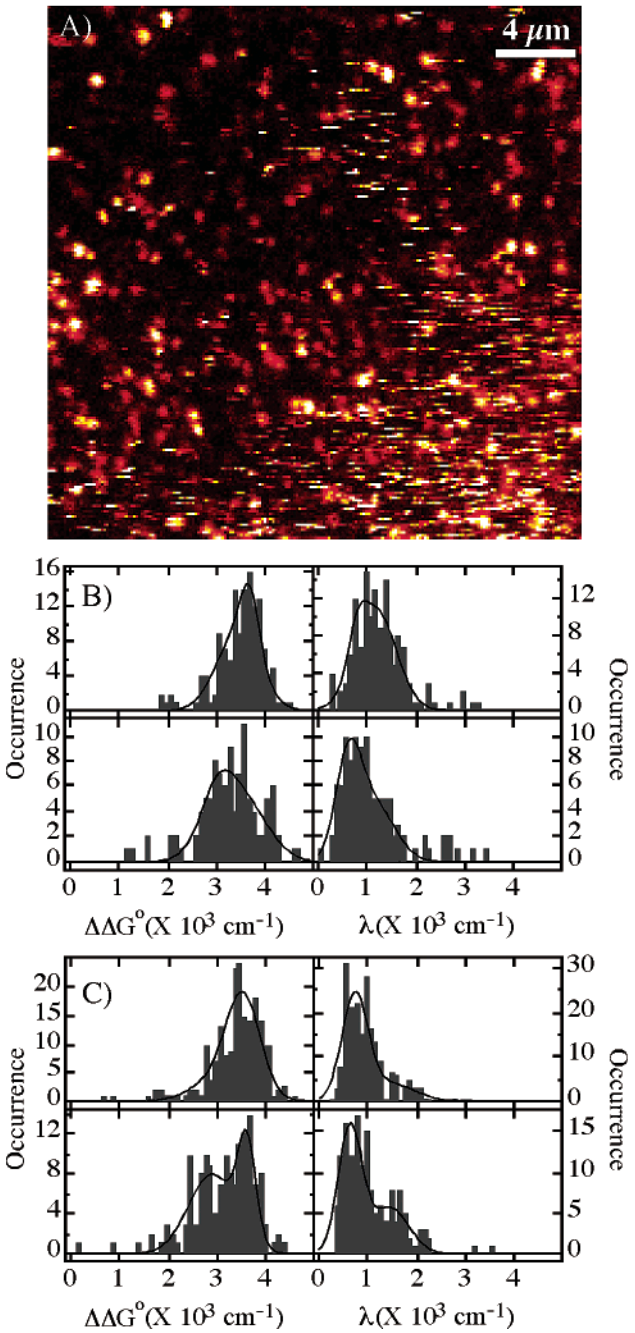

Figure 7. Comparison of films prepared from cohydrolyzed and separately hydrolyzed sols. (A) Image of sample prepared by mixing separately hydrolyzed CNS, BTMOS, and TEOS immediately prior to film casting. The image provides strong evidence for phase separation of the components. Rapid molecular diffusion occurs in the lower right portion of the image where fluorescent streaks are depicted. (B) $\Delta\Delta G°$ and λ histograms for films containing 50% CNS and 50% TEOS prepared by (top) cohydrolysis of the materials and (bottom) mixing of separately hydrolyzed 50% CNS and 50% TEOS sols. (C) $\Delta\Delta G°$ and λ histograms for films containing 25% CNS, 25% BTMOS, and 50% TEOS prepared by (top) cohydrolysis of all materials and (bottom) mixing of separately hydrolyzed 50% CNS/TEOS and 50% BTMOS/TEOS sols. Also shown in the histograms in B and C are fits to double-Gaussian functions as in Figure 3.

appearance of such fluctuations indicates that these environments are more fluid, leading to time-dependent changes in the single-molecule excitation and/or emission properties.

The above observations provide conclusive evidence of micrometer-scale phase separation of organic-rich and inorganic-rich domains in the separately hydrolyzed materials. Clearly, relatively more fluid organic regions are formed along with more rigid, highly crosslinked inorganic domains. Observation of micrometer-scale phase separation and micrometer-sized fluid domains does not require the use of single-molecule experiments. However, these results provide information on the possible origins of the signal fluctuations and image streaks seen in other samples as well. It is concluded here that the image streaks observed for individual molecules in images such as that shown in Figure 1 also result from the presence of fluid environments. These fluid environments are clearly much smaller than those depicted in images such as the one shown in Figure 7. Indeed, the fluctuations in this case might instead result from the presence of nanometer-scale fluid domains.

Although the above imaging results point to clear phase separation of silicate materials, they also point to the difficulties associated with obtaining single-molecule spectroscopic data from such samples. Whereas molecules entrapped in fixed film locations can be probed, single-molecule spectra cannot be obtained from film regions in which the molecules are rapidly diffusing. However, some separately hydrolyzed samples that exhibited relatively little image streaking could be characterized.

Figure 7B shows data from films prepared by separate hydrolysis of CNS and TEOS. The two sols were mixed in a 1:1 ratio immediately prior to film casting. Few image streaks were observed, leading to the conclusion that the vast majority of molecules were entrapped in fixed locations in this sample. This behavior contrasts with that observed for similarly prepared 50% BTMOS films. In these samples, substantial imaging streaking was observed, along with a reduced number of fixed, round fluorescent spots. Again, these differences are attributed to the different miscibilities of CNS and BTMOS materials with TEOS.

The data in Figure 7B clearly exhibit differences between the separately and cohydrolyzed CNS/TEOS samples. The $\Delta\Delta G°$ distribution for the separately hydrolyzed material is peaked at slightly lower values and is also broader than that obtained for the cohydrolyzed materials. The broadening of the $\Delta\Delta G°$ distribution reflects the expected increase in sample heterogeneity.[49] The shift in the distribution to smaller $\Delta\Delta G°$ values suggests that the most prevalent environments in these films are somewhat less polar than those in the cohydrolyzed films. The average $\Delta\Delta G°$ for the distribution is 3300 ± 130 cm^{-1}. For the cohydrolyzed materials, it is 3440 ± 85 cm^{-1}. The error bars given are the 95% confidence limits for each value. The slightly decreased polarity of the film environments in the separately hydrolyzed materials is most likely due to the presence of CNS-rich domains. The highly polar TEOS-rich environments observed in the samples of low organic content (see Figure 3), however, are not observed. It is likely that the dramatically weaker fluorescence obtained from NR in TEOS-rich environments biases the distribution toward CNS-rich regions.

Interestingly, the λ distribution is also peaked at smaller values for the separately hydrolyzed materials,

although a long tail to large values is also observed. The shift to smaller λ values results from entrapment of the molecules in relatively less polar and more rigid film environments. In the cohydrolyzed 50% CNS samples, the environments are molecularly mixed, relatively polar, and relatively fluid. The greater polarity results from the incorporation of Si−O−Si and Si−OH functionalities. In the separately hydrolyzed materials, the CNS-rich environments might be encapsulated in more rigid TEOS film regions, resulting in a simultaneous increase in rigidity and a decrease in polarity. This hypothesis is consistent with the shift to smaller $\Delta\Delta G°$ values in the separately hydrolyzed materials.

Films prepared from BTMOS, CNS, and TEOS in a 1:1:2 ratio were also characterized. As noted above, results from separately hydrolyzed BTMOS, CNS, and TEOS were excluded because of the problems associated with fast diffusion in the organic-rich domains. However, films prepared by mixing separately hydrolyzed 50% BTMOS and 50% CNS sols in a 1:1 ratio yielded films that showed little evidence of molecular diffusion. Figure 7C displays plots of the data obtained from cohydrolyzed and separately hydrolyzed materials. As with the 50% CNS samples, the $\Delta\Delta G°$ distribution for the separately hydrolyzed materials is broadened and its average is shifted to smaller values, compared to the distribution obtained for the cohydrolyzed samples. The data reflect the incorporation of 50% CNS and 50% BTMOS regions in the films, making these samples distinctly more heterogeneous than the cohydrolyzed materials. Indeed, the observed distribution is similar to that obtained by summing the data from the 50% CNS and 50% BTMOS samples shown in Figure 3. It is noteworthy that the λ and $\Delta\Delta G°$ distributions for the separately hydrolyzed materials appear to be bimodal. Such an observation likely reflects the presence of BTMOS-rich and CNS-rich domains. In the cohydrolyzed materials, single distributions are observed, suggesting molecular-scale mixing of the three film components.

Finally, the λ distributions for the cohydrolyzed and separately hydrolyzed mixtures shown in Figure 6C exhibit trends consistent with those of the 50% CNS samples. The peaks of the distributions are centered at similar values for the two samples, reflecting the presence of environments of moderate polarity and fluidity. However, the distribution for the separately hydrolyzed materials shows a greater population of molecules exhibiting large λ values. The apparent increase in the population of these sites is likely due to the presence of polar, fluid 50% CNS-rich domains. Again, a similar λ distribution can be obtained by summing the distributions for the corresponding 50% samples reported in Figure 3. As a result, these data are consistent with the presence of phase-separated domains of 50% CNS and 50% BTMOS.

IV. Conclusions

In summary, silicate thin films prepared from sols containing different mole fractions of inorganic (TEOS) and organic (BTMOS and CNS) silanes have been studied using single-molecule spectroscopic methods. The data obtained have yielded valuable new information on the nanoscale properties of these materials and the origins of material heterogeneity. Local matrix polarity and rigidity were explored as a function of sol composition. Rigid, polar environments were found in all films of low organic content. As the organic content increased, the films were observed to become distinctly less polar and less rigid. Most interesting were the differences observed in the trends toward less polar, less rigid environments in the CNS and BTMOS sample series. The CNS samples exhibited a gradual shift in properties with increasing organic content, whereas the BTMOS materials exhibited an abrupt change in properties for films of approximately 50% BTMOS content. These different behaviors were attributed to differences in the miscibility of the precursor species, with CNS being much more miscible with TEOS.

Of most importance to those seeking to develop devices from this class of materials, the single-molecule data clearly show important differences between the average and most common film environments. In the majority of the samples investigated, the most common environments were found to be more polar than the average. Similarly, the most common environments were also observed to be distinctly more rigid than the average. It is the most common environments that are of greatest importance in understanding and optimizing the chemistry of silicate films. However, such information is often obscured in the bulk spectroscopic measurements most often employed in their characterization.

The single-molecule methods described here represent valuable new analytical tools that will be useful to those developing silicate materials for a number of technological applications. Using these methods to characterize newly designed materials, it might be possible to develop devices for which the most common (rather than the average) environments are tailored to have properties best suited to their specific applications. For example, by incorporation of organic functionality into silicate materials using different precursors, thin films with tailored polarity and rigidity properties can be prepared. Materials that more readily interact with polar and/or nonpolar species can also be designed. Last, by the appropriate selection of precursors having different miscibilities, films incorporating nanoscale phase-separated organic and inorganic domains could also be obtained. Single-molecule spectroscopic methods promise to continue providing new information important to the complete understanding of these useful but complex materials.

Acknowledgment. The authors thank Rachel Allenbaugh and Prof. Anne M. Kelley for their contributions to this work. Funding was provided by the Army Research Office (DEPSCoR) and Kansas State University.

Supporting Information Available: Two figures showing the raw ν_{fl} and $\delta\nu_{fl}$ data used in the preparation of Figures 3 and 7 (PDF). This material is available free of charge via the Internet at http://pubs.acs.org.

CM020344J